JMEPEG (2023) 32:4295–4305
https://doi.org/10.1007/s11665-022-07404-0

1059-9495/$19.00

TECHNICAL ARTICLE

On the Heat Treatment of Selective-Laser-Melted 316L

Iuliia Morozova, Christian Kehm, Aleksei Obrosov, Yitong Yang, Kamal Uddin Mohammad Miah, Elena Uludintceva, Sebastian Fritzsche, Sabine Weiß, and Vesselin Michailov

Submitted: 21 June 2022 / Revised: 30 July 2022 / Accepted: 20 August 2022 / Published online: 29 September 2022

The effect of heat treatment at various temperatures (650, 850, 1050, and 1100°C) and dwell times (10 min and 1 h) on the metallurgical and microstructural evolution as well as on the related tensile properties of stainless steel 316L processed by selective laser melting (SLM) has been systematically evaluated. The metallurgical and microstructural features such as defects, stability of the columnar–cellular structure and substructure, second phase particles, and phase transformation imparted by SLM and heat treatment have been discussed. It has been shown that the processing conditions specific to SLM significantly alter the kinetics of phase evolution compared to standard welding techniques which affects the accuracy of the prediction. The influence of these characteristics on tensile properties and hardness was elucidated. It was disclosed that with increasing heat treatment temperature there was a gradual increase in elongation but a decrease in strength related to the dislocation density and the development of the microstructure.

Keywords 316L, grain structure, heat treatment, phase evolution, SLM, tensile properties

1. Introduction

316L austenitic stainless steel has a wide range of applications in several industries, particularly in corrosive environments, such as oil and gas, marine, chemical, biomedical, and nuclear energy industries. Recently, it has been extensively processed by selective laser melting (SLM) for manufacturing of structural components with complex geometry, superior mechanical properties, and corrosion resistance. The specific columnar–cellular microstructure inherited by SLM, combined with the appropriate process parameters to provide high-density parts, can result in superior strength and ductility of printed 316L, comparable or better than these of conventionally manufactured counterparts (Ref 1-3).

Even though an excellent combination of strength and ductility of the 316L components can be achieved by SLM, the mechanical and functional properties, especially ductility, can suffer due to inevitable metallurgical defects such as pores, lack of bonding, large residual stresses, coarse columnar structure, and elemental segregation (Ref 2, 4). Heat treatment can be applied to the as-printed parts to overcome the mentioned issues. Extensive research to the influence of post-processing heat treatment on the microstructural transformation (Ref 5-8), tensile properties (Ref 9, 10), wear behavior (Ref 4, 11), fatigue properties (Ref 12-14), corrosion resistance (Ref 15, 16), and impact toughness (Ref 17) of the SLM printed 316L has been extensively researched to date.

Currently, there is no consensus on the microstructural evolution and the alternation of the mechanical properties with different heat treatments of SLM fabricated 316L. In general, the hardness and both, the tensile and the yield strength decreased with increasing heat treatment temperature, due to the reduction of dislocation density, disappearance of cellular substructures, and grain growth (Ref 18-21). However, there are a number of studies that show a variety of mechanical properties depending on the treatment conditions. For instance, Montero Sistiaga et al. (Ref 17) reported that heat-treated SLM 316L exhibited comparable tensile strength at all annealing temperatures while the yield strength decreased at higher temperatures of 950 and 1095°C. Similarly, N. Chen et al. (Ref 22) achieved a 10% increase in yield strength by annealing at 400°C due to the additional formation of nano-sized silicates. A higher UTS after heat treatment than the one in the as-welded condition is reported by Leuders et al. (Ref 12).

One of the controversial issues is the effect of heat treatment on the ductility of the printed 316L. Many studies reported an increase in elongation of various degrees (Ref 4, 18, 21). K. Saeidi et al. (Ref 10) observed that the elongation of samples annealed at 1100°C increased by about 7% compared to the as-built samples. A similar heat treatment applied by W. S. Shin et al. (Ref 4) significantly increased the elongation of the samples printed with various SLM parameters. According to Ref 19, the ductility of SLM printed 316L increased regressively with increasing heat treatment temperature. Maximum values of elongation of 51.6% (25.2% more than the as-printed value), 54.7% (*i.e.*, + 34%) and 57.5% (*i.e.*, + 26.4%) were achieved by heat treatment at 1200°C for 2 h (Ref 16), 1100°C for 0.5 h (Ref 4), and 1100°C for 5 min (Ref 20), respectively. Some studies (Ref 16, 17, 20) highlighted that the uniform elongation started to improve at higher temperatures of 1100°C while at lower temperatures there was no change or even

Iuliia Morozova, Christian Kehm, Kamal Uddin Mohammad Miah, Sebastian Fritzsche, and **Vesselin Michailov**, Department of Joining and Welding, Brandenburg University of Technology Cottbus-Senftenberg, 03046 Cottbus, Germany; **Aleksei Obrosov, Yitong Yang, Elena Uludintceva,** and **Sabine Weiß**, Department of Metallurgy and Materials Technology, Brandenburg University of Technology Cottbus-Senftenberg, 03046 Cottbus, Germany. Contact e-mails: moroziu1@b-tu.de, Kehm@b-tu.de, aleksei.obrosov@b-tu.de, yitong.yang@b-tu.de, miah@b-tu.de, uludiele@b-tu.de, fritzseb@b-tu.de, weiss@b-tu.de, and michailov@b-tu.de.

deterioration. This trend as well as the large standard deviation of the elongation values were attributed by Montero Sistiaga and co-workers (Ref 17) to the presence of oxides inclusions.

A negative effect of heat treatment on the elongation of the printed 316L was also reported (Ref 9, 22, 23). According to Ref 9, elongation remained unchanged and even dropped at lower temperatures (below 600°C) and higher temperatures up to 1400°C, respectively. The material treated at 400 and 800°C consistently exhibited a loss of elongation compared to the as-built one (Ref 22).

Taken together, these studies indicate that heat treatment has great potential to improve the elongation of SLM processed 316L. However, the evidence on its influence is inconsistent, which complicates the selection of the heat treatment parameters to achieve the required property level. In the present study, 316L was processed by SLM and subsequently heat-treated at various temperatures and dwell times to increase the elongation for medical application. Therefore, the study aims to systematize the knowledge by accompanying the obtained results with a critical review of data from published studies.

2. Experimental

2.1 Material

Gas atomized 316L stainless steel powder (m4p material solutions GmbH, Germany) with a particle size ranging between 15 and 45 μm was used for the present study. The particle distribution of the powder was as follows: D10 = 21.1, D50 = 30.1, D90 = 41.4 μm. The powder consisted of spherical- particles with some smaller satellite particles attached, as shown in Fig. 1. The chemical composition of the as-received powder is listed in Table 1.

2.2 SLM Process

The specimens for the study were produced in the SLM125-Realizer machine (Realizer GmbH, Germany) equipped with a 400 W fiber laser with a wavelength of 1070 nm. The smallest spot of the laser beam in the focal plane is 30 μm in diameter. The building volume of the machine is 12.5 cm × 12.5 cm × 20.0 cm. The tensile specimens were built in vertical orientation in argon atmosphere with a maximum oxygen content of 0.15%. The geometry was selected according to DIN 50,125 (Ref 24), as presented in Fig. 2a. These specimens were used for the microstructural observations and the hardness measurement (Ref 24).

The 316L specimens were printed on a stainless steel 316L substrate plate. Layer thickness, laser power, and scanning speed were set at 50 μm, 150 W, and 1000 mm/s, respectively. The melting line distance in the layer (hatch distance) was 80 μm. The "chessboard" strategy was applied where the stripes had a width of 5 mm and a length of 10 mm with an overlap of 0.02 mm. Each layer was rotated at an angle of 27° with respect to the previous one, as shown in Fig. 2b.

2.3 Post-processing Heat Treatment

The cylindrical tensile specimens were mechanically separated from the platform, which was alleviated by support structures with a length of 4 mm. This ensured the separation of the samples without the introduction of mechanical stresses.

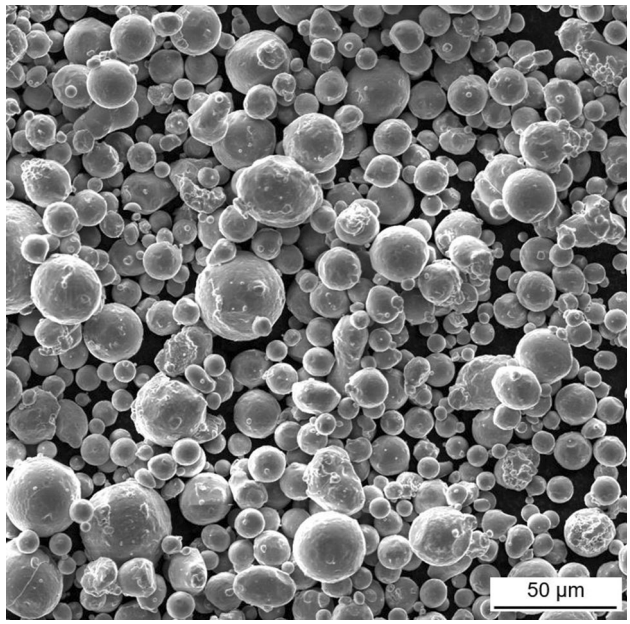

Fig. 1 SEM image of the 316L powder subjected to SLM

Table 1 Chemical composition of the as-received powder in wt. %

C	Si	Mn	Ni	Cr	Mo	Fe
0,02	0,7	1,1	11,1	17,0	2,3	Basis

The printed specimens were not subjected to any mechanical operations before heat treatment. The post-processing heat treatment was performed in a Nabertherm furnace of Fischer Scientific GmbH (Schwerte, Germany) under argon atmosphere. It was carried out at holding temperatures of 650, 850, 1050, and 1100°C for 10 min and 1 h. The treated samples were cooled to room temperature in air while those treated at 1050°C were additionally water quenched to study the influence of the cooling medium on the behavior of the second phase. All heat treatment conditions are summarized in Table 2 presented in Results and Discussion.

2.4 Microstructural and Mechanical Characterization

The samples for the microstructural investigations and hardness measurements were cut from the center of the tensile specimens parallel to the build direction using a slow-speed diamond saw under water cooling, as illustrated in Fig. 2c. The position of the samples was chosen so that the microstructure could be examined directly in the gauge area and correlated with the mechanical properties. Subsequently, the samples were prepared for optical microscopy (OM) by a multi-step metallographic procedure with a final polishing step of 0.05 μm and etched with the V2-Beize reagent heated to 60°C for 10 s.

Porosity was analyzed on the polished unetched samples in the transverse and longitudinal directions relative to the build direction (see Fig. 2c). It was subsequently characterized by image analysis and measured by means of ImageJ software (Version 1.53 k, National Institutes of Health, USA). The area fraction of porosity was determined from ten images in each

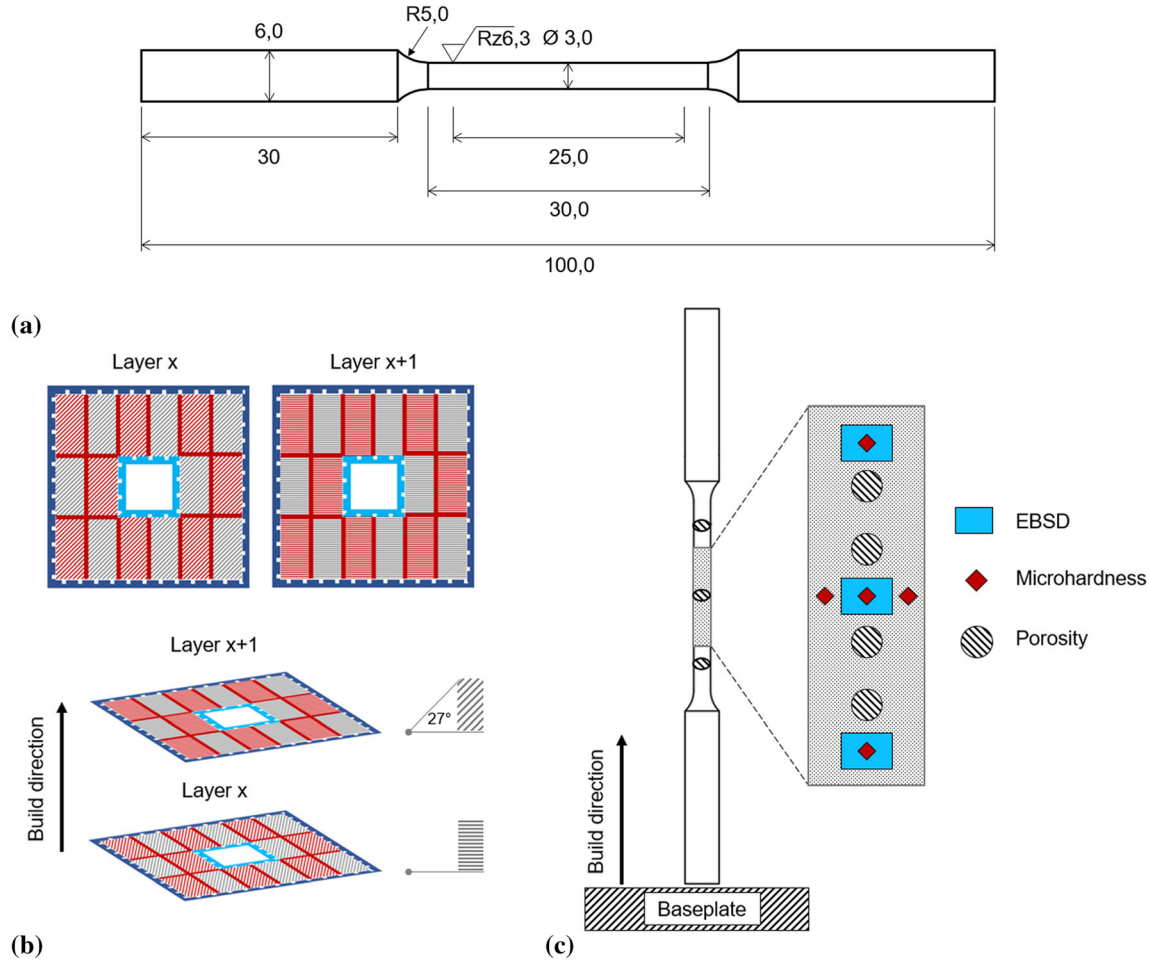

Fig. 2 (a) Geometry of the printed specimens; (b) printing strategy; and (c) location of sampling for the microstructural investigations and hardness measurement

Table 2 Mechanical properties of 316L as-printed and heat-treated under various conditions

Processing condition	Defect fraction, %	Hardness, HV 1	Yield strength YS, MPa	Ultimate tensile strength UTS, MPa	Elongation ε, %
As-printed	0.43	231	444	638	38,8
650°C, 10 Min, air	0.41	226	464	635	34,0
650°C, 1 h, air	0.47	215	452	631	36,4
850°C, 10 Min, air	0.39	207	406	605	40,6
850°C, 1 h, air	0.51	204	397	610	44,9
1050°C, 10 Min, air	0.29	193	372	593	47,9
1050°C, 1 h, air	0.24	186	337	577	49,6
1050°C, 10 min, water	0.35	187	354	583	47,8
1050°C, 1 h, water	0.43	188	308	560	50,8
1100°C, 10 Min, air	0.52	187	346	583	46,7
1100°C, 1 h, air	0.67	166	283	552	50,2

orientation taken at different locations, and the results obtained were averaged.

The characterization of the microstructure and the second phase particles was performed with the scanning electron microscope (SEM) TESCAN MIRA II (Brno, Czech Republic) equipped with an INCA Oxford detector for energy-dispersive x-ray spectroscopy (EDS) and with the confocal 3D laser scanning microscope type KEYENCE VK-X1000 type (Neu-Isenburg, Germany).

Electron backscatter diffraction (EBSD) analysis was performed using the EDAX EBSD system (AMETEK Materials Analysis Division, Mahwah, NJ, USA) with a step size of 0.4 μm. TSL-OIM (AMETEK Materials Analysis Division, Mahwah, NJ, USA) software was used for the analysis. Inverse pole figure (IPF) maps with a minimum confidence index (CI) of 0.2 were produced for each area investigated. A lower-boundary misorientation angle of 2° was used to eliminate the noise effect.

The Vickers microhardness was measured on both, the as-printed and the heat-treated samples with a load of 9.807 N (HV 1) for 15 s. The results of five measurements on each sample were used to estimate an average value. Tensile tests were carried out at room temperature on an Instron ElectroPuls E10000 tensile testing machine (Norwood, USA) which has a maximum linear static capacity of 7 kN. The crosshead speeds during the tensile test were selected according to DIN EN ISO 6892-1 (Ref 25). The specimens were not machined before the test. The tests were performed up to the rupture of the specimens. The mechanical properties (ultimate tensile strength, yield stress, and elongation) were determined as average values of five specimens.

3. Results and Discussion

3.1 As-welded State

3.1.1 Density. Table 2 shows the area percentage of defects consisting mainly of pores and lack of fusion (in %). As follows from the data, the SLM parameters applied to 316L resulted in manufacturing of dense parts ($>$ 99.5%). It should be noted that the density was higher in the cross section than in the longitudinal section of the printed samples which can be attributed to a higher area fraction of "lack of fusion" defects between the separate melt pools. The pore size varied from a few micrometers to a maximum size of $\sim$ 50 μm.

3.1.2 Grain Structure. Figure 3 demonstrates a columnar–cellular structure typical for the material processed by SLM. The columnar grains of a wide size range are aligned with the build direction and some of them grew epitaxially through the melt pools, reaching a width of $\sim$ 30 μm and a length of $\sim$ 100 μm. The proportion of high-angle grain boundaries (HAGBs) significantly outweighs that of low-angle grain boundaries (LAGBs), as determined by EBSD (the corresponding IPF map is shown in Fig. 5a).

The SEM image taken at higher magnification (Fig. 3c) revealed equiaxed cells with a size $\sim$ 0.6 μm inside the columnar grains. It is now well established from a large number of studies that dislocation tangles, which arise in large quantities due to the rapid solidification rate of up to 10^7 K/s typical for SLM, are concentrated at the cell boundaries (Ref 26, 27). Interestingly, Y. M. Wang and co-workers (Ref 3) demonstrated that these dislocation walls do not generate local misorientations at the boundaries but within the cells. Therefore, they cannot be treated as subgrains, but are strong obstacles to dislocation movement.

The cell boundaries were decorated with bright spots. The contrast indicates that the spots were enriched in Mo and Cr which tend to segregate due to their low solubility in the austenitic matrix and rapid solidification rate. The enrichment of the cell walls with Cr and Mo as well as with Si and Mn observed in many works was explained by the rapid solidification (Ref 1, 3, 7, 16). Hence, the cell boundaries can be regarded as chemical segregations within a homogeneous matrix.

3.1.3 Second Phases. It is known that 316L tends to form various second phases through rich alloying (Ref 28). However, the rapid solidification during SLM suppresses the precipitation of inclusions. Inherently, nano-sized particles containing O, Si, and Al (also Mn, Cr, and N) are usually present in the as-printed 316L (Ref 10, 16, 20, 26). A variety of the compositions are reported so these particles are variously referred to as silicon oxide (Ref 29), Si-O-Mn silicates (Ref 22), amorphous Mn-Si-rich precipitates (Ref 9), oxynitrides of Ti, Al, and Mo (Ref 23), $MnSiO_3$ particles (Ref 27). Nano-oxide inclusions are typically observed at cell boundaries and are thought to have some strengthening effect (Ref 27, 29). In addition, W. S. Shin et al. (Ref 4) detected fine $M_{23}C_6$ carbides by optical and SEM observations; however, their chemical composition was not measured.

In the current study, the particles were observed in the structure of the as-welded 316L (blue inclusions in Fig. 4). They were found to form as oxidation products during etching. These particles were not introduced into the structure by the SLM process and were therefore not considered relevant to the properties of the SLM parts. Otherwise, no particles were found in the as-printed microstructure.

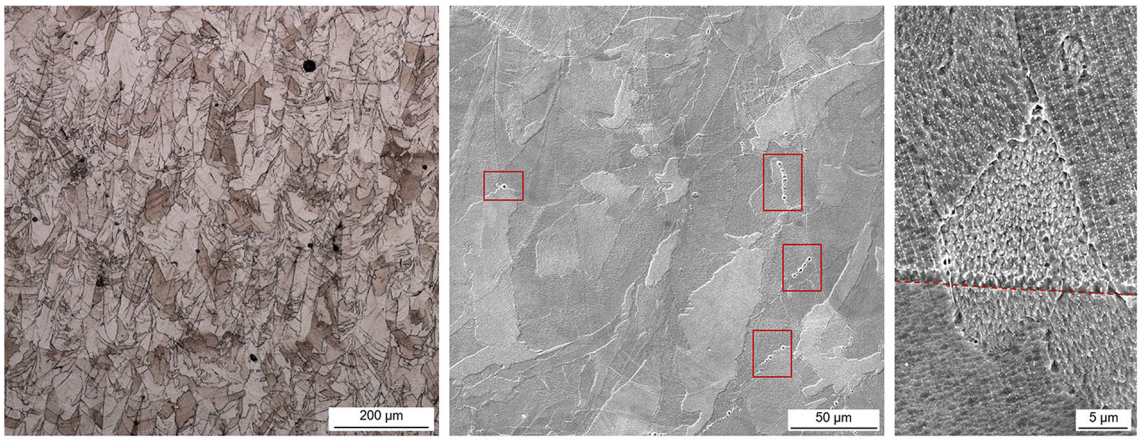

Fig. 3 Columnar–cellular structure of the as-printed 316L microstructure: (a) light optical overview image; (b) SEM overview image (red rectangles highlight the inclusions of δ-ferrite); and (c) SEM image of fine cells inside the columnar grains (red dotted line represents the melt pool boundary)

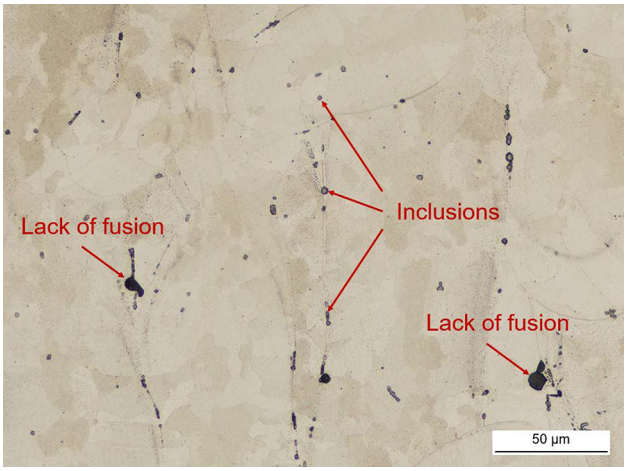

Fig. 4 Laser scanning image indicating oxide particles on the surface of as-printed 316L

3.1.4 Phase Composition. It is known that the austenitic structure of molten 316L can undergo a partial transformation of austenite to δ-ferrite according to the ternary Fe-Cr-Ni diagram at 70% Fe (Ref 28). Three analyses have been used to date to determine the phase composition of selective-laser-melted 316L: optical or SEM observations, EBSD, and x-ray diffraction (XRD) techniques. The majority have found that the as-welded microstructure is pure austenite (Ref 2, 4, 10, 29). In contrast, a small amount of δ-ferrite was reported by K. Saeidi et al. (Ref 26) using EBSD analysis which was considered more reliable compared to XRD. Furthermore, the presence of ferrite has been obtained by microstructural investigations in Ref 1, 5, 8, 23; however, with such small δ-amounts this seems to be an uncertain technique, considering the variety of etching techniques and their influence on the determination of microstructural constituents. Thus, the question of phase composition remains controversial.

In the present work, phase analysis by EBSD was carried out on the bottom, middle, and top of the sample in the as-welded state to show the possible difference due to the different thermal conditions. It was assumed that the multiple re-heating may promote the formation of δ-ferrite, which means that a higher fraction of ferrite should be found at the bottom of the sample. However, the volume fraction of ferrite was 0.002, 0.006, and 0.005 in the lower, middle, and upper part of the sample, respectively. A measurement error has to be taken into account because the defects are calculated as ferrite. Figure 5b shows the distribution of the phases at the top of the sample. As can be seen, there was only an insignificant amount of δ-ferrite along the dendrite boundaries, which is supported by the segregation of ferrite-promoting elements such as Mo and Cr. Thus, Kurzynowski et al. (Ref 23) associated the intercellular micro-segregation of Cr, Si, and Mo with the formation of eutectic δ-ferrite. The precipitation of ferrite stabilizers also supports the formation of single austenite. Some traces of δ-ferrite were observed in SEM analysis (red rectangles in Fig. 3b) as these inclusions were rich in Cr and Mo. Therefore, a negligible amount of ferrite is homogeneously distributed within the austenitic matrix of as-printed 316L.

The predicted ferrite content for as-welded 316L according to the WRC-1992 diagram is 6 FN (ferrite number), as shown in Fig. 6. According to the Technical Report ISO/TR 22,824 (Ref 30), the error range of the diagram is about ± 4 FN in the range from 0 to 18 FN, so the predicted range is between 2 and 10 FN. 316L has mixed ferrite–austenite solidification mode that allows avoiding hot cracking. Indeed, the SLM processed parts were crack-free despite being almost fully austenitic. This can be explained by the bead geometries and volumes of the deposits produced by SLM which are favorable to reduce restraint stresses and thus avoid cracking. The absence of δ-ferrite has shown that SLM conditions involving rapid heating and solidification significantly alter phase evolution compared to standard welding techniques and therefore require new tools for the prediction of phase composition.

It is important to emphasize that this work was carried out with a specific and single batch 316L powder while there are applicable composition ranges for 316L material. The amount of austenite-promoting elements versus ferrite-promoting elements and the specific levels of trace elements such as sulfur and phosphorus in the feedstock material used could have an influence on the solidification mode, the appearance of hot cracks, or the occurrence of intermetallic phases (Ref 31). Therefore, systematic investigations should confirm whether higher or lower Cr_{eq}/Ni_{eq} ratios have an influence on the microstructure and structure soundness of the deposits obtained with SLM.

3.2 Heat-Treated State

In the present study, the purpose of heat treatment was to increase the elongation of the SLM processed 316L. The parameters were selected based on literature data from the following points of view: annealing at 650°C was to relieve stresses; 850°C temperature was applied to reduce stresses and maintain the favorable cellular structure; the temperature of 1050°C was to dissolve potential detrimental second phases (water cooling suppresses their re-formation) and avoid the formation of δ-ferrite; heating at 1100°C was performed to check the possibility of phase transformation.

3.2.1 Density. The defects inherited by the SLM process such as porosity and lack of fusion are a vital factor affecting the fracture behavior and mechanical properties of the SLM printed parts. In the present study, it can be concluded that the heat treatment has no effect on the density of the SLM parts, as follows from Table 2. No relationship was identified between the area fraction of defects and the heat treatment parameters. The analysis of the unetched macrographs revealed that the number of very small pores with a size of a few micrometers increased after heat treatment which did not influence the values calculated on the basis of size. This could be due to oxidation during heating even though argon was used. This result is in agreement with that of Ronneberg et al. (Ref 19) and Chao et al. (Ref 20). However, E. Tascioglu et al. (Ref 11) found that the porosity of the SLM parts was gradually reduced by increasing the heat treatment temperature due to the homogenization of the structure. Similarly, in Ref 4, the number of defects such as partially molten particles and pores was reduced by the heat treatment. In Ref 5, 16 even the opposite is stated: the heat treatment had a detrimental effect on the porosity.

3.2.2 Grain Structure. Figure 7 and 8 shows the microstructures of the as-printed samples heat-treated for 10 and 60 min, respectively. As can be seen, the melt pool boundaries inherited from the SLM gradually disappear due to

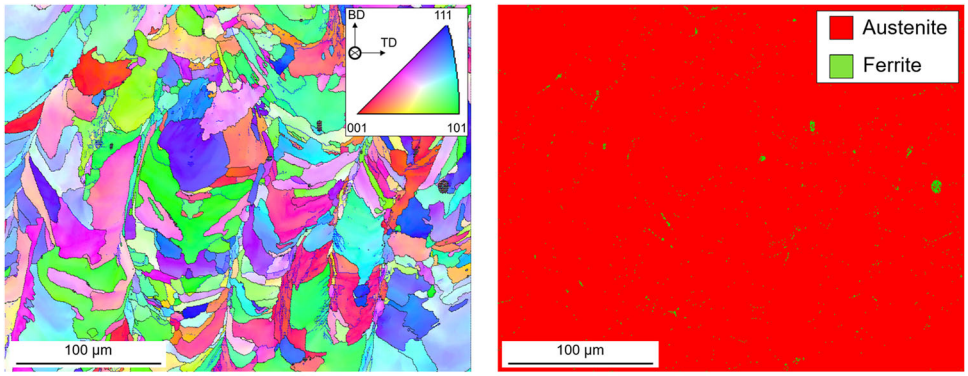

Fig. 5 (a) IPF map combined with grain boundaries distribution (blue lines represent LAGBs) and (b) corresponding phase composition at the top of the as-printed 316L

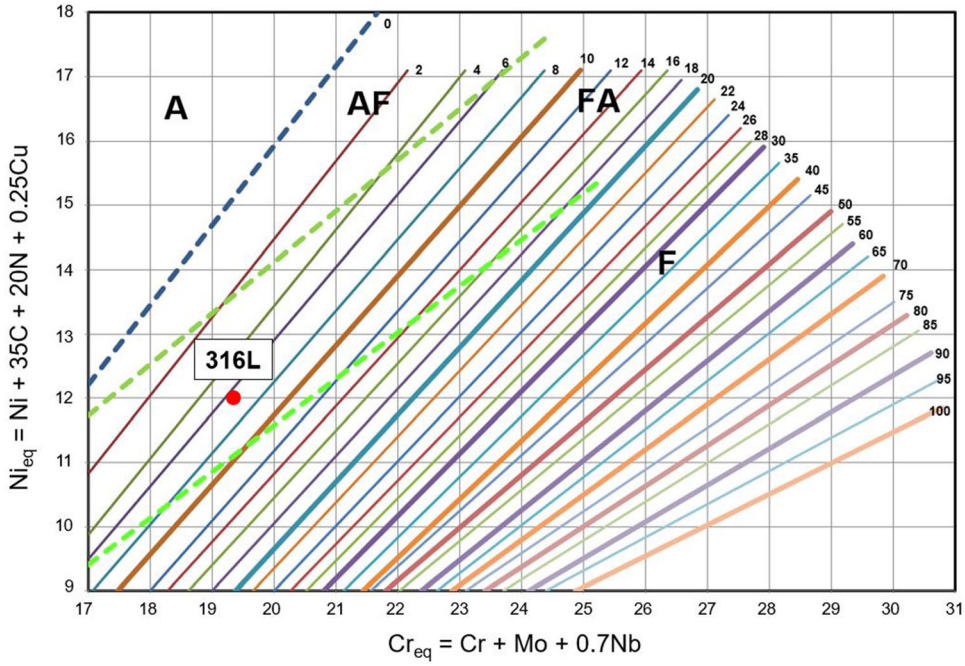

Fig. 6 Position of as-welded 316L on the WRC-1992 diagram [28]

the treatment at 850°C for both 10 and 60 min. They are no longer visible in the structure heated at 1050°C while the coarse grains still remain. The phenomenon of disappearance of melt pool boundaries during heat treatment is reported in the literature as a result of atomic diffusion from approx. 600°C (Ref 8, 9, 11, 16, 17, 20). The size of the columnar grains gradually increased when treated up to 1050 °C which is consistent with previous studies (Ref 4, 9, 16, 20). However, according to the studies (Ref 17, 19), the microstructure was not subjected to grain enlargement by heating up to 1040-1095°C but at higher temperatures. A comparison between the grain size in the as-welded and in the condition treated at 1100°C is not possible, as there was a significant transformation of the grain structure at this temperature.

According to previous findings, the cellular structure begins to disappear when heated above 400°C (Ref 22) or rather above ~ 600°C due to rearrangement or annihilation of dislocations and diffusion of elements until complete dissolution at 1000-1100°C. At the same time, progressive coarsening was observed (Ref 19, 20, 23). In the present study, the cellular structure was found to have high thermal stability as it was still visible after heating at 1100°C for 1 h (Fig. 9b). For instance, the cellular microstructures were no longer observed in the as-printed material heated at 1100 °C for 6 h (Ref 9). It outlines that the dwell time has as important impact as the temperature regarding the survival of cells. As can be seen in Fig. 9b, there are segregations of Mo and Cr at the cell boundaries, but their fraction was considerably lower than that in the as-printed state. It is believed that slow dissolution of Mo and Cr provides a pinning effect that preserves the cellular structure up to very high temperatures. D. Kong et al. (Ref 32) have associated the high thermal stability of the cellular structures with relatively low stored energy in the SLM printed material, The cells had an elongated shape in contrast to the equiaxed cells in the as-built state; however, this could be a consequence of the different growth direction of a columnar grain in which the cells were

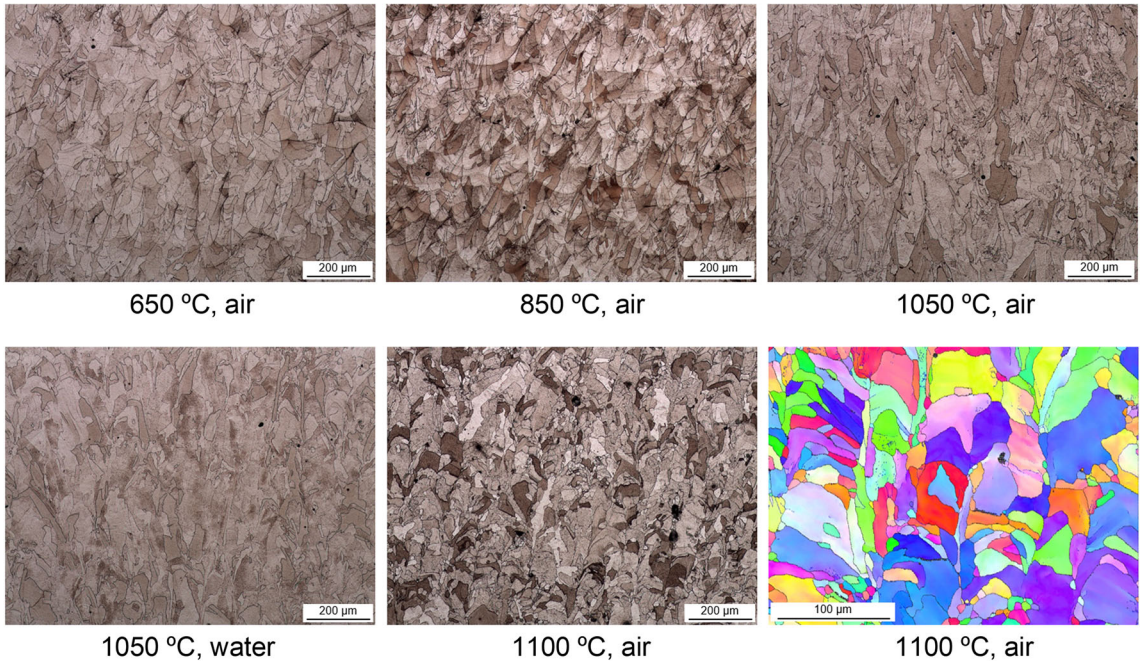

Fig. 7 Microstructure of the samples annealed for 10 min

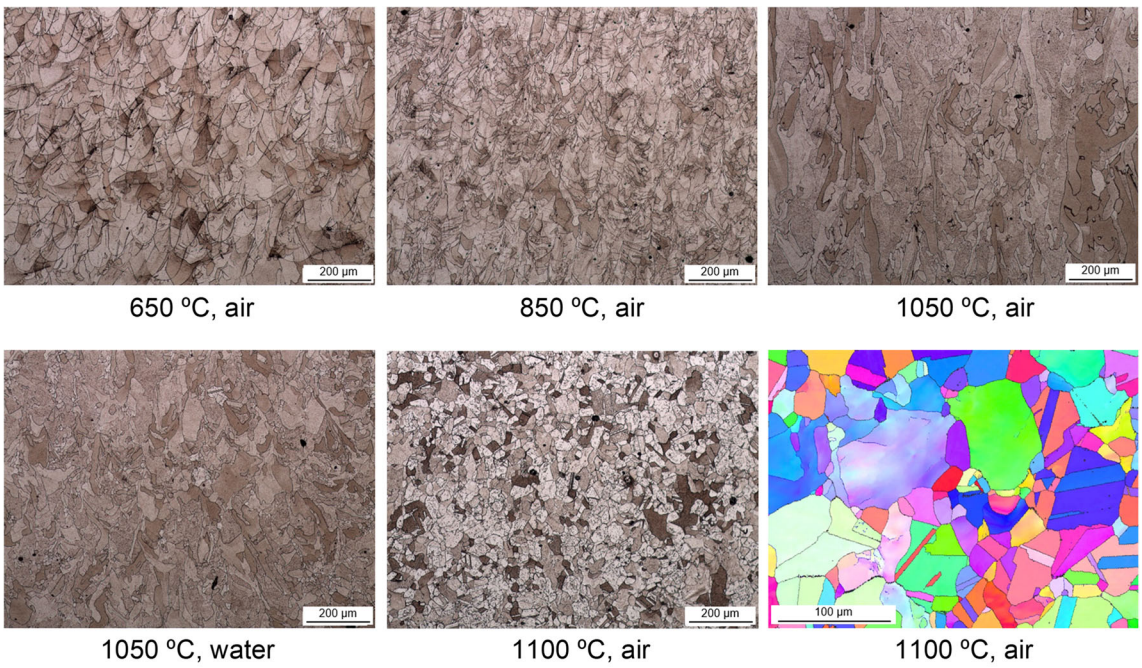

Fig. 8 Microstructure of the samples annealed for 60 min

located (Ref 32). Comparison with the original cell size suggests that the growth of the cells did not occur during heat treatment, but progressive dissolution (Fig. 9). The structure was homogenized by treatment at 1100°C for a dwell time of 60 min eliminating microstructural anisotropy. However, the refinement of the grains was inhomogeneous, and the grain size varied widely from 2 to 80 μm. Interestingly, recrystallized grains as well as twin grains were observed in the sample treated at 1100°C for 60 min (particularly noticeable in the IPF map in Fig. 8) while no such formation was observed in the structure treated for 10 min. The large differences in grain size can be explained by different mechanisms of grain evolution such as fusion of initial grains and cells, recrystallization, growth of recrystallized grains, and twinning. Annealing twins of various morphologies were predominantly located within the recrystallized grains. Apparently, heating at 1100°C for 10 min was not sufficient to initiate the recrystallization process.

The SLM conditions lead to a high concentration of dislocations both at the sub-cell boundaries and inside the cells. Their distribution is uneven because the cells are concentrated inside the grains with different dimensions and orientations depending on the cooling conditions. Therefore,

some SLM grains are more suitable for recrystallization which requires high dislocation density together with temperature. This leads to a random appearance of recrystallized grains in the structure. The recrystallized grains are favorable for twinning. According to Y. Jin et al. (Ref 33), the formation of the annealing twins in austenitic stainless steel is more intense at the beginning of recrystallization and not during grain growth. The crucial role of the previous strain level in the generation of the annealing twin density was also highlighted. Therefore, it can be assumed that the appearance of the twins marks the formation of the recrystallized grains. Once the growth of newly formed recrystallized grains had started, the formation of the twins was inhibited.

A number of studies report the rearrangement of the coarse columnar grains into an equiaxed grain structure at temperatures of 1200°C and above or at 1110°C for a longer dwell time of 8 h (Ref 16, 17, 20). Similarly, the twinning phenomenon is reported to occur at a temperature of 1400°C (Ref 9, 10) or at a temperature of 1100°C for a longer time of 8 h (Ref 20). This variety of reported temperatures can be explained by different initial strain conditions, *i.e.*, the density of dislocations in the as-printed material, which in turn is determined by the process parameters.

3.2.3 Second Phases. Even though the evolution of nano-sized inclusions present in the as-printed 316 structure during heat treatment has been extensively studied, it remains controversial. A change in the chemical composition upon heat treatment was detected in several studies (Ref 16, 20, 27, 34). For instance, D. Kong and co-workers revealed a depletion of aluminum from O-Al-Si-(Ti, Mn) nanoinclusions (Ref 16) or decreased content of Mn and Si in complex MnSi inclusions (Ref 34). It was shown that a size of nano inclusions increased (Ref 20, 27) or decreased (Ref 34) during heat treatment. N. Chen et al. (Ref 22) observed an increase in the volume fraction of Si-O-Mn silicates in the SLM structure annealed at 400°C as well as proposed a partial dissolution at higher temperature of 800°C. Dissolution of smaller Mn-Si-rich particles was also revealed by Salman et al. (Ref 9). It can be concluded that these processes are governed by the chemical composition of inclusions due to various solubility of the elements contained.

Coarse oxide inclusions found in the SLM structure in the present work were stable during heat treatment. However, as they originate from etching and do not affect the mechanical properties, they are not further discussed.

Otherwise, no phases, especially no detrimental σ-phase were found after heat treatment. In contrast, the precipitation of σ-phase and its precursors during heat treatment has been demonstrated in a few studies (Ref 4, 20, 23). W. S. Shin et al. (Ref 4) suggested that the σ-phase occurred inside the grains owing to the transformation from δ-ferrite while Q. Chao et al. (Ref 20) proposed the precipitation mechanism from precursors in a temperature range of 650-800°C although the as-built structure was free of ferrite which is usually required for the formation of σ-phase.

3.2.4 Phase Composition. As -printed 316L was found to consist of austenite with a negligible amount of δ-ferrite. Heat treatment at all temperatures had no effect on the phase composition. This is in agreement with the results of previous researchers where temperatures up to 1400°C were used (Ref 3, 6, 13). Furthermore, S. Waqar et al. (Ref 18) have outlined that the cooling rate does not destabilize the austenite phase. However, the conclusion on the effect of heat treatment on the phase composition obviously depends on the initial phase composition of the as-printed structure. For instance, M S I N Kamariah et al. (Ref 8), who detected some amount of δ-ferrite in the SLM fabricated parts, reported the reduction of the δ-ferrite fraction when the temperature was raised to 1100°C.

One of the controversial issues is the possibility of phase transformation during heat treatment at 1100°C. In the present study, heat treatment at 1100°C for both, 10 and 60 min resulted in no phase transformation, as shown in Fig. 10. This finding is consistent with Q. Chao et al. (Ref 20) who were able to detect a nano-sized lath-like δ-phase in the material treated at 1400°C while a fully austenitic structure was maintained at 1100°C and various holding times.

This contrasts with the earlier studies by Saeidi et al. (Ref 10) where δ-ferrite was detected in the samples treated at 1100°C for 6 min by XRD, EBSD analysis, and was even observed in the TEM images in the form of fine needles. It was assumed that an increase in Cr equivalent due to the dissolution of Mo during heating lowers the minimum transformation temperature. The chemical composition of the powder used in the current study was largely the same as that used in the study (Ref 10). The Mo content of 2.3 was the same. Considering that the austenite-ferrite transformation starts at ∼ 1260 °C for the given Cr and Ni equivalents according to the Fe-Cr-Ni ternary diagram (Ref 28), it is hard to imagine that the dissolution of Mo (or other ferrite-promoting elements) can shift the transformation temperature to 1100°C. It should be noted again that the Cr_{eq}/Ni_{eq} ratio can be decisive in each individual case.

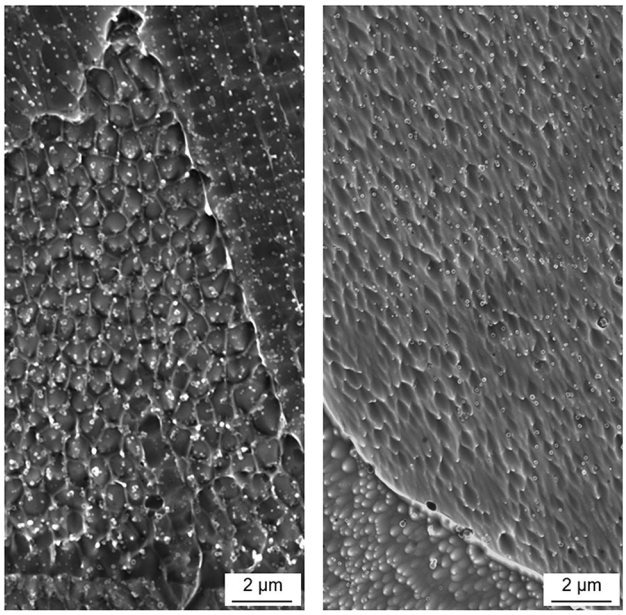

Fig. 9 Cellular structure (a) as-printed and (b) treated at 1100 °C for 60 min (air cooling) state

3.3 Mechanical Properties

3.3.1 Hardness. Table 2 compares the results of the hardness measurements. There is a clear tendency for hardness to decrease with increasing heat treatment temperature, which is consistent with previously reported results (Ref 4, 8, 11, 16). In

some work, heat treatment-induced softening of selective-laser-melted 316L started at higher temperatures (Ref 8, 17). A significant reduction of the dislocation density, *i.e.*, the residual stresses as well as the disappearance of melt pool boundaries and the columnar–cellular structure were cited as reasons for the decreasing hardness. In addition, the reduced volume fraction of δ-ferrite due to heat treatment is also said to be responsible for softening (Ref 8).

Since the pure austenitic phase was present in all as-welded and heat-treated samples, the phase composition was not relevant for the hardness. It is known that the columnar–cellular structure effectively impedes dislocation motion which strengthens the SLM manufactured material. The results have shown that the cells gradually dissolved during heat treatment even though they still exist at high temperatures (Fig. 9b). The evolution of the substructure with increasing temperature can be tracked by the fraction of LAGBs. For example, the fraction of LAGBs in the as-printed material was 0.248 for a total length of 5.86 mm while the heat treatment at 1100 °C drastically reduced it to 0.182 for a total length of 2.97 mm after 10 min and to 0.125 for a total length of 1.58 mm after 60 min. This indicates that the developed dislocation network was considerably degraded during the heat treatment resulting in a continuous decrease in hardness with increasing temperature.

Interestingly, the water cooling slowed down the further hardness decrease due to the treatment at 1050°C which could be explained by the introduction of thermal stresses into the material due to the rapid cooling.

3.3.2 Tensile Properties. Table 2 summarizes the results of the tensile test and is supplemented by Fig. 11 which graphically illustrates the correlation between the mechanical properties and the heat treatment temperature. Both the yield and the tensile strength decrease gradually while the elongation increases with increasing heat treatment temperature. The exception to this tendency was the treatment at 650°C which increased the yield strength and decreased the elongation while the UTS was almost the same as for the as-printed specimen.

Defects are a crucial factor for the fracture behavior of SLM parts. The improvement of mechanical properties by heat treatment due to the reduction of the number of defects has been discussed by E. Tascioglu et al. (Ref 11) and Shin et al. (Ref 4). However, in the current study, no influence of the heat treatment on the density was found which excludes this factor. The defects, such as the lack of fusion cannot be altered by temperature because they sharply reduce the density of the SLM parts, unlike the pores. The analysis of the defects showed that small pores were introduced during the heat treatment which should not notably deteriorate the strength and ductility.

Overall, the decrease in strength with increasing heat treatment temperature is associated with the reduction in dislocation density and coalescence of the cell substructure. The role of the cells in the fracture behavior was emphasized by Y. Zhong et al. (Ref 29) who found that the size of the dimples on the fracture surface is directly dependent on the cell size in the as-manufactured microstructure. Chao et al. (Ref 20) analyzed many factors with respect to the change in mechanical properties due to heat treatment such as stress relief, coarsening of columnar grains and inclusions, phase transformation, and the formation of secondary phases or precipitates. Substructure evolution including dislocations density and cell size was identified as the cause of yield strength reduction, while the impact of grain growth was neglected. Reduction in ductility was partially attributed to coarsening of oxide inclusions. As follows from the data on the fraction and length of LAGBs (see section Hardness), the dislocation concentration was significantly lower inside the cells, although their boundaries slowly dissolved as they were pinned by segregated elements. The melt pool and columnar grain boundaries, which are also obstacles to dislocations, disappeared at lower heat treatment temperatures in contrast to the cells. Although the cells survived at high temperatures, the significant reduction in dislocation density primarily led to a reduction in the strength of the material.

Elongation reached its maximum value after heat treatment both at 1100°C for one hour and at 1050°C for one hour followed by water cooling. The homogenized microstructure together with twins in the case of the material treated at 1100°C as well as the reduced dislocation density contributed to the enhancement of the elongation. This is in line with the study of Ronneberg et al. (Ref 19) which showed a positive effect of annealing, involving the elimination of the anisotropy, in the mechanical properties by dissolving the melt pool boundaries and the inhomogeneous columnar–cellular structure. Based on this observation, annealing was proposed as a measure to suppress the failure tendency along the boundaries. It should be noted that the remaining cellular structure should positively affect the elongation. For instance, in the study of Liu et al. (Ref 1), a scenario was proposed in which the cell walls impede the dislocation movement but do not stop it completely. As a

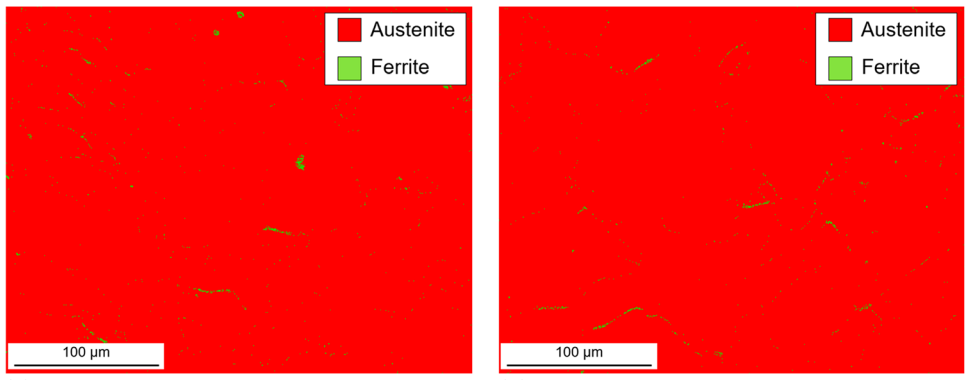

Fig. 10 Phase composition of the samples heat-treated at 1100 °C for (a) 10 min and (b) 60 min

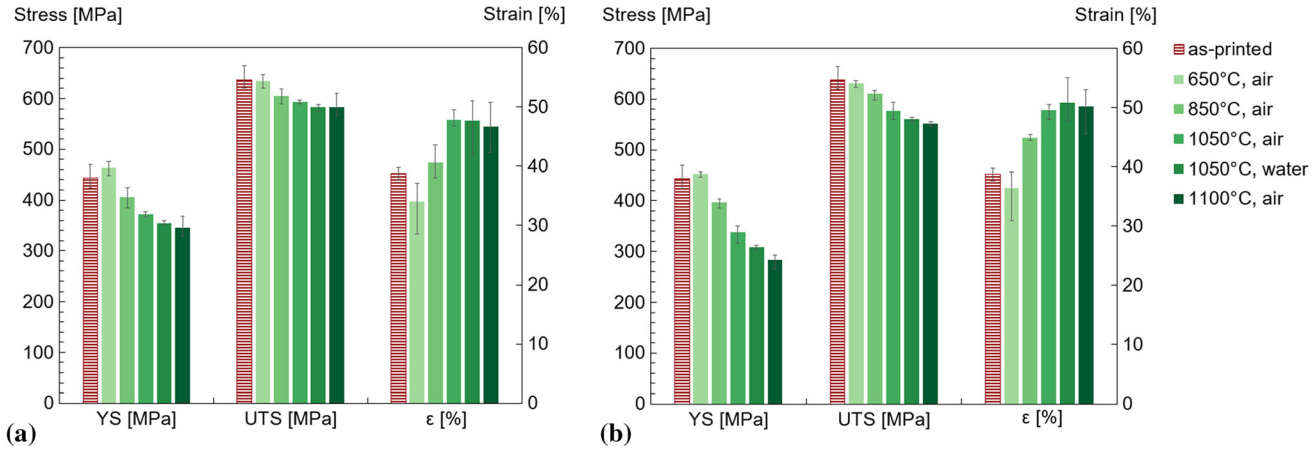

Fig. 11 Tensile properties of as-printed 316L and heat-treated for (a) 10 min and (b) 60 min

result, the strength is increased but not at the expense of ductility.

As mentioned above, annealing at 650°C increased the yield strength but decreased the elongation. It could be assumed that the precipitation of the σ-phase is responsible for this behavior. According to Chao and co-workers (Ref 20), the formation of the σ-phase at 650-800°C resulted in a remarkable loss of ductility together with a coarsening of the Mn-Si-O oxides at the austenite grain boundaries. Nevertheless, it is hard to believe that a significant σ-formation took place as the yield strength did not suffer but the appearance of fine precursors such as chi (χ) phase can be deduced.

4. Conclusions

The aim of the present work was to improve the elongation of 316L printed by selective laser melting (SLM) which was required for numerous applications, including biomedical purposes. The effects of heat treatment with different temperatures and dwell times on microstructural evolution and mechanical performance under static loading were systematized. Based on the results the following conclusions were drawn:

1. A single-phase austenite with a negligible amount of δ-ferrite was formed along the entire section of the SLM-produced parts. The as-printed phase composition remained stable during heat treatment at all temperatures up to 1100°C.
2. The complex structure originating from the SLM process showed different thermal stability during heat treatment. The melt pool boundaries and the columnar grains disappeared at 850°C and 1050°C, respectively, while the fine cellular structure was still visible after a one-hour annealing at 1100°C.
3. No second phase particles were observed in both, the as-printed and the heat-treated microstructures.
4. Elongation increased strongly with increasing heat treatment temperature while both yield strength and tensile strength decreased. Defects such as pores and lack of fusion were not affected by the heat treatment so the density of the SLM parts was not a decisive factor for the mechanical characteristics. The phase composition was also not decisive, as it was retained during heat treatment. A significant decrease in dislocation density, especially within the cells, reduced the strength of the material.
5. The improvement in elongation by heat treatment at 850–1100°C was associated with the reduced dislocation density, homogenization of the grain structure, and surviving cells. Treatment at lower temperatures cannot ensure the absence of detrimental precursors.

Funding

Open Access funding enabled and organized by Projekt DEAL.

References

1. L. Liu, Q. Ding, Y. Zhong, J. Zou, J. Wu, Y.-L. Chiu, J. Li, Z. Zhang, Q. Yu, and Z. Shen, Dislocation Network in Additive Manufactured Steel Breaks Strength–Ductility Trade-Off, *Mater. Today*, 2018, **21**(4), p 354–361. https://doi.org/10.1016/j.mattod.2017.11.004
2. D. Wang, C. Song, Y. Yang, and Y. Bai, Investigation of Crystal Growth Mechanism During Selective Laser Melting and Mechanical

Property Characterization of 316L Stainless Steel Parts, *Mater. Des.*, 2016, **100**, p 291–299. https://doi.org/10.1016/j.matdes.2016.03.111
3. Y.M. Wang, T. Voisin, J.T. McKeown, J. Ye, N.P. Calta, Z. Li, Z. Zeng, Y. Zhang, W. Chen, T.T. Roehling, R.T. Ott, M.K. Santala, P.J. Depond, M.J. Matthews, A.V. Hamza, and T. Zhu, Additively Manufactured Hierarchical Stainless Steels with High Strength and Ductility, *Nat. Mater.*, 2018, **17**, p 63–71
4. W.S. Shin, B. Son, W. Song, H. Sohn, H. Jang, Y.-J. Kim, and C. Park, Heat Treatment Effect on the Microstructure, Mechanical Properties, and Wear Behaviors of Stainless Steel 316L Prepared via Selective Laser Melting, *Mater. Sci. Eng. A*, 2021 https://doi.org/10.1016/j.msea.2021.140805
5. J. Kluczyński, L. Snie·zek, K. Grzelak, A. Oziębło, K. Perkowski, J. Torzewski, I. Szachogłuchowicz, K. Gocman, M. Wachowski, and B. Kania, Comparison of Different Heat Treatment Processes of Selective Laser Melted 316L Steel Based on Analysis of Mechanical Properties. *Materials*, 2020, doi: https://doi.org/10.3390/ma13173805
6. K. Saeidi, M. Neikter, J. Olsen, Z.J. Shen, and F. Akhtar, 316L Stainless Steel Designed to Withstand Intermediate Temperature, *Mater. Des.*, 2017, **135**, p 1–8. https://doi.org/10.1016/j.matdes.2017.08.072
7. L. Cui, S. Jiang, J. Xu, R.L. Peng, R.T. Mousavian, and J. Moverare, Revealing Relationships Between Microstructure and Hardening Nature of Additively Manufactured 316L Stainless Steel, *Mater. Des.*, 2021 https://doi.org/10.1016/j.matdes.2020.109385
8. M. S. I. N. Kamariah, W. S. W. Harun, N. Z. Khalil, F. Ahmad, M. H. Ismail, and S. Sharif, Effect of Heat Treatment on Mechanical Properties and Microstructure of Selective Laser Melting 316L Stainless Steel. In: IOP Conference Series: Materials Science and Engineering, (2017), vol. 257, no. 1. doi: https://doi.org/10.1088/1757-899X/257/1/012021
9. O.O. Salman, C. Gammer, A.K. Chaubey, J. Eckert, and S. Scudino, Effect of Heat Treatment on Microstructure and Mechanical Properties of 316L Steel Synthesized by Selective Laser Melting, *Mater. Sci. Eng., A*, 2019, **748**, p 205–212. https://doi.org/10.1016/j.msea.2019.01.110
10. K. Saeidi, X. Gao, F. Lofaj, L. Kvetková, and Z.J. Shen, Transformation of Austenite to Duplex Austenite-Ferrite Assembly in Annealed Stainless Steel 316L Consolidated by Laser Melting, *J. Alloy. Compd.*, 2015, **633**, p 463–469. https://doi.org/10.1016/j.jallcom.2015.01.249
11. E. Tascioglu, Y. Karabulut, and Y. Kaynak, Influence of Heat Treatment Temperature on the Microstructural, Mechanical, and Wear Behavior of 316L Stainless Steel Fabricated by Laser Powder Bed Additive Manufacturing, *Int. J. Adv. Manuf. Technol.*, 2020, **107**(5–6), p 1947–1956. https://doi.org/10.1007/s00170-020-04972-0
12. S. Leuders, T. Lieneke, S. Lammers, T. Tröster, and T. Niendorf, On the Fatigue Properties of Metals Manufactured by Selective Laser Melting - The Role of Ductility, *J. Mater. Res.*, 2014, **29**(17), p 1911–1919. https://doi.org/10.1557/jmr.2014.157
13. B. Blinn, M. Klein, C. Gläßner, M. Smaga, J.C. Aurich, and T. Beck, An Investigation of the Microstructure and Fatigue Behavior of Additively Manufactured AISI 316L Stainless Steel with Regard to the Influence of Heat Treatment, *Metals*, 2018 https://doi.org/10.3390/met8040220
14. O. Fergani, A.B. Wold, F. Berto, V. Brotan, and M. Bambach, Study of the Effect of Heat Treatment on Fatigue Crack Growth Behaviour of 316L Stainless Steel Produced by Selective Laser Melting, *Fatigue Fract. Eng. Mater. Struct.*, 2018, **41**(5), p 1102–1119. https://doi.org/10.1111/ffe.12755
15. K. Wang, Q. Chao, M. Annasamy, P.D. Hodgson, S. Thomas, N. Birbilis, and D. Fabijanic, On the Pitting Behaviour of Laser Powder Bed Fusion Prepared 316L Stainless Steel Upon Post-processing Heat Treatments, *Corros. Sci.*, 2022 https://doi.org/10.1016/j.corsci.2021.110060
16. D. Kong, C. Dong, X. Ni, L. Zhang, J. Yao, C. Man, X. Cheng, K. Xiao, and X. Li, Mechanical Properties and Corrosion Behavior of Selective Laser Melted 316L Stainless Steel After Different Heat Treatment Processes, *J. Mater. Sci. Technol.*, 2019, **35**(7), p 1499–1507. https://doi.org/10.1016/j.jmst.2019.03.003
17. M. L. Montero Sistiaga, S. Nardone, C. Hautfenne, and A. van Humbeeck, Effect of Heat Treatment of 316L Stainless Steel Produced by Selective Laser Melting (SLM). In: Proceedings of the 27th Annual International Solid Freeform Fabrication Symposium - An Additive Manufacturing Conference, pp. 558–565, (2016)
18. S. Waqar, J. Liu, Q. Sun, K. Guo, and J. Sun, Effect of Post-heat Treatment Cooling on Microstructure and Mechanical Properties of Selective Laser Melting Manufactured Austenitic 316L Stainless Steel, *Rapid Prototyp. J.*, 2020, **26**(10), p 1739–1749
19. T. Ronneberg, C.M. Davies, and P.A. Hooper, Revealing Relationships Between Porosity, Microstructure and Mechanical Properties of Laser Powder Bed Fusion 316L Stainless Steel Through Heat Treatment, *Mater. Des.*, 2020 https://doi.org/10.1016/j.matdes.2020.108481
20. Q. Chao, S. Thomas, N. Birbilis, P. Cizek, P.D. Hodgson, and D. Fabijanic, The Effect of Post-processing Heat Treatment on the Microstructure, Residual Stress and Mechanical Properties of Selective Laser Melted 316L Stainless Steel, *Mater. Sci. Eng. A*, 2021 https://doi.org/10.1016/j.msea.2021.141611
21. H.D. Carlton, A. Haboub, G.F. Gallegos, D.Y. Parkinson, and A.A. MacDowell, Damage Evolution and Failure Mechanisms in Additively Manufactured Stainless Steel, *Mater. Sci. Eng., A*, 2016, **651**, p 406–414. https://doi.org/10.1016/j.msea.2015.10.073
22. N. Chen, G. Ma, W. Zhu, A. Godfrey, Z. Shen, G. Wu, and X. Huang, Enhancement of an Additive-Manufactured Austenitic Stainless Steel by Post-Manufacture Heat-Treatment, *Mater. Sci. Eng., A*, 2019, **759**, p 65–69. https://doi.org/10.1016/j.msea.2019.04.111
23. T. Kurzynowski, K. Gruber, W. Stopyra, B. Kuźnicka, and E. Chlebus, Correlation Between Process Parameters, Microstructure and Properties of 316 L Stainless Steel Processed by Selective Laser Melting, *Mater. Sci. Eng., A*, 2018, **718**, p 64–73. https://doi.org/10.1016/j.msea.2018.01.103
24. DIN 50125:2016–12. Testing of metallic materials –Tensile test pieces, 2016
25. "Metallic materials - Tensile testing - Part 1: Method of Test at Room Temperature (ISO 6892–1:2019); German version EN ISO 6892–1:2019."
26. K. Saeidi, X. Gao, Y. Zhong, and Z.J. Shen, Hardened Austenite Steel with Columnar Sub-grain Structure Formed by Laser Melting, *Mater. Sci. Eng., A*, 2015, **625**, p 221–229. https://doi.org/10.1016/j.msea.2014.12.018
27. F. Yan, W. Xiong, E. Faierson, and G.B. Olson, Characterization of Nano-scale Oxides in Austenitic Stainless Steel Processed by Powder Bed Fusion, *Scripta Mater.*, 2018, **155**, p 104–108. https://doi.org/10.1016/j.scriptamat.2018.06.011
28. J. C. Lippold, and D. J. Kotecki, Welding Metallurgy and Weldability of Stainless Steels. 5th ed. John Willey & Sons, USA (2005), 376 pages. ISBN: 978–0–471–47379–4
29. Y. Zhong, L. Liu, S. Wikman, D. Cui, and Z. Shen, Intragranular Cellular Segregation Network Structure Strengthening 316L Stainless Steel Prepared by Selective Laser Melting, *J. Nucl. Mater.*, 2016, **470**, p 170–178. https://doi.org/10.1016/j.jnucmat.2015.12.034
30. "Welding consumables - Predicted and Measured FN in Specifications-A position Statement of the Experts of IIW Commission IX," 2003
31. P.S. Korinko, and S.H. Malene, Considerations for the Weldability of Types 304L and 316L Stainless Steels, *Practical Failure Analysis and Prevention*, 2001, **1**(4), p 41–68. https://doi.org/10.1007/BF02715336
32. D. Kong, C. Dong, S. Wei, X. Ni, L. Zhang, R. Li, L. Wang, C. Man, and X. Li, About Metastable Cellular Structure in Additively Manufactured Austenitic Stainless Steels, *Addit. Manuf.*, 2021, **38**, 101804. https://doi.org/10.1016/j.addma.2020.101804
33. Y. Jin, M. Bernacki, G.S. Rohrer, A.D. Rollett, B. Lin, and N. Bozzolo, Formation of Annealing Twins During Recrystallization and Grain Growth in 304L Austenitic Stainless Steel, *Mater. Sci. Forum*, 2013, **753**, p 113–116. https://doi.org/10.4028/www.scientific.net/MSF.753.113
34. D. Kong, X. Ni, C. Dong, L. Zhang, C. Man, J. Yao, K. Xiao, and X. Li, Heat Treatment Effect on the Microstructure and Corrosion Behavior of 316L Stainless Steel Fabricated by Selective Laser Melting for Proton Exchange Membrane Fuel Cells, *Electrochim. Acta*, 2018, **276**, p 293–303. https://doi.org/10.1016/j.electacta.2018.04.188